

# Influence of the regioregularity on the chiral supramolecular organization of poly(3-alkylsulfanythiophene)s.

Helmuth Peeters<sup>a</sup>, Pauline Couturon<sup>a</sup>, Steven Vandeleene<sup>a</sup>, David Moerman<sup>b</sup>, Philippe Leclère<sup>b</sup>, Roberto Lazzaroni<sup>b</sup>, Inge De Cat<sup>c</sup>, Steven De Feyter<sup>c</sup> and Guy Koeckelberghs<sup>a\*</sup>

Received (in XXX, XXX) Xth XXXXXXXXXX 20XX, Accepted Xth XXXXXXXXXX 20XX

DOI: 10.1039/b000000x

The manuscript investigates the influence of the regioregularity (RR) of poly(3-alkylsulfanythiophene)s (P3AST) on their properties. Therefore, a series of P3ASTs (**P1-P5**) with different RR was synthesized using a combination of a “reversed McCullough method” and the GRIM method. The degree of RR was determined by <sup>1</sup>H NMR spectroscopy. A detailed chiroptical study in good solvent, poor solvent and film was performed, which revealed that the tendency to form chiral supramolecular aggregates clearly depends on the RR, but that the relation is not simply continuously increasing. Instead, the strongest effects were observed in P3ASTs with high, but not 100% RR. As a consequence, a similar behaviour can be expected for a regioregular and an irregular P3AST. This hypothesis was tested on a regioregular and an irregular P3AST that proved to have similar chiroptical properties in a previous study. Their properties in the solid state were investigated into detail using STM and AFM.

## Introduction

The remarkable optical, electrical and electronic properties of conjugated polymers depend to a large extent on their supramolecular organization. Often a lamellar supramolecular organization is preferred, in which the  $\pi$ -conjugated backbones stack face-to-face. The major driving force for this stacking are  $\pi$ -interactions. In addition, VDW interactions between (ordered) side-chains within the alkyl-phase might aid the stacking process. A typical example of a conjugated polymer that shows this lamellar structure, is regioregular, head-to-tail coupled poly(3-hexylthiophene) (P3HT). The material, despite its rather simple molecular structure, owes its extraordinary properties to this supramolecular organization. If poly(3-alkylthiophene)s (P3ATs) are substituted with linear (achiral) alkyl groups, the polymer chains stack parallel, while the use of chiral alkyl groups results in the chiral, helical stacking of the polymer chains and the appearance of concomitant chiral effects, such as circular dichroism (CD)<sup>1,5</sup> and circularly polarized luminescence<sup>4</sup>, enantioselective cyclic voltammetry<sup>6</sup> and second-harmonic generation-circular dichroism<sup>7</sup>. In such mono-substituted polythiophenes a regioregular, head-to-tail placement of the (alkyl)substituent is of great importance. First, since the regular molecular structure associated with the regular placement of the substituent might contribute to the formation of the supramolecular structure. Second, the head-to-head (HH)-couplings, inevitably present in regio-irregular P3ATs, result in a nonplanar conformation, which prevents a close packing of the polymer chains and therefore complicates the formation of the supramolecular organization. Indeed, regio-irregular P3ATs consisting of a large amount of non-head-to-tail (HT)-couplings do not organize into lamellae and have poor optical and electronic properties<sup>3</sup>. The influence of the RR on the crystallinity has recently been investigated<sup>8</sup>.

The reason why a HH-dyad in P3ATs results in a nonplanar conformation, is the bulkiness of the group directly attached to the polymer backbone (*i.e.* methylene, Vanderwaals (VDW) radius = 2.0 Å). If, however, this group is replaced by a smaller group (O-atom, VDW radius = 1.4 Å or S-atom, VDW radius = 1.8 Å), the steric hindrance is smaller and a planar conformation becomes

possible. This is nicely exemplified in regioregular HH-TT-coupled poly(thiophene)s. HH-TT poly(3-alkoxythiophene) (P3AOT)<sup>9</sup> and HH-TT P3AST<sup>10</sup> form a lamellar supramolecular structure which, if chiral substituents are employed, show strong CD effects, while HH-TT P3ATs do not form such structure at all. As already mentioned, regio-irregular P3ATs does not organize into a lamellar structure and neither do regio-irregular P3AOTs, as is expressed by the significant lower CD effects<sup>11</sup> and Faraday rotation<sup>12</sup>, although the presence of HH-couplings do not hinder the formation of a planar conformation in the latter polymers. Peculiarly, we have found that the supramolecular behavior of regioregular HT-P3AST and a particular regio-irregular P3AST hardly differs from each other<sup>13</sup>. Indeed, the only difference – albeit small – was  $\lambda_{\max}$  in good solvent, reflecting the presence of HH-couplings in the regioirregular P3AST, which disrupt the conjugation of the polymer backbone. The UV-vis and CD spectra in a poor solvent mixture or in film are essentially the same and clearly point at chiral stacking. Also the DSC data (T<sub>m</sub>,  $\Delta H$ ) show great similarities. From these data, it must be concluded that both P3ASTs organize into the same, chiral supramolecular structure, which is in strong contrast to other conjugated polymers.

To elucidate whether the regioregularity does not affect the properties of P3AST, we synthesized a series of P3ASTs with different degree of RR and investigated into detail how the RR affects the supramolecular structure of P3ASTs. In a second part, we performed an in-depth characterization of the previously prepared regioregular and regio-irregular P3AST using scanning tunneling microscopy (STM) and atomic force microscopy (AFM) to obtain real space visualization.

## Results and Discussion

### Polymer synthesis and characterization

A series of P3ASTs of approximately the same molar mass, but different RR were prepared. This was accomplished using Ni(dppp)Cl<sub>2</sub> as a catalyst while varying the isomeric purity of the monomer feed (*i. e.* 2-bromo-3-alkylsulfanyl-5-bromomagnesiothiophene **2b** and 2-bromo-4-alkylsulfanyl-5-

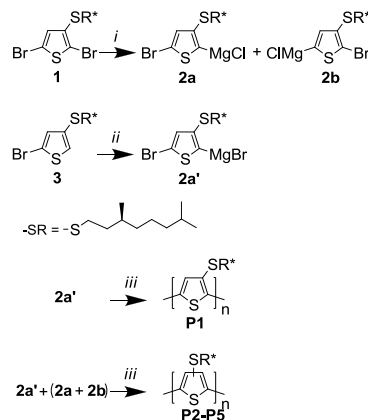
halomagnesiothiophene **2a** and **2a'**). Indeed, while the use of Ni(dppp)Cl<sub>2</sub> in case of P3ATs results in HT-P3ATs even if both isomers are present by effectively preventing the formation of a HH-coupling<sup>27</sup>, this is not the case for P3ASTs. This can again be correlated to the reduced size of a S-atom compared with a methylene group. Instead, both isomers – if both present – are consumed<sup>13</sup>. Consequently, the RR of P3ASTs can be tuned by varying the isomeric purity in the feed. The monomers are prepared in two ways. A mixture of both isomers is prepared via a Grignard Metathesis (GRIM) reaction on 2,5-dibromo-3alkylsulfanylthiophene using *i*-PrMgCl, resulting in **2a** and **2b** in an approximately 1.1/1 ratio (Scheme 1). For HT-P3ASTs, either pure **2a** or **2b** is required. Since **2b** is prone to scrambling, resulting again in a mixture of isomers, **2a'** was preferred, which was synthesized in a McCullough-like procedure starting from **3**. In order to vary the isomeric purity in the feed, the monomer solutions – both from the GRIM and the ‘reversed McCullough’ method – were mixed in different ratios and Ni(dppp)Cl<sub>2</sub> was added, resulting in **P1-P5**. The ratio (**2a'**+**2a**+**2b**)/Ni(dppp)Cl<sub>2</sub> was kept approximately constant at 35/1. After polymerization, the crude polymer was precipitated in methanol, isolated and further purified via Soxhlet extractions with acetone and hexanes for **P1-P3** and acetone and pentane for **P4-P5**. Finally all polymers were extracted with chloroform, concentrated, precipitated in methanol and dried in vacuo.

The number averaged molar mass ( $\overline{M}_n$ ) and polydispersity (D) of the polymers **P1-P5** were determined by GPC in THF toward polystyrene standards. The molar mass of the polymers (Table 1) concurs reasonably well.

The RR, as was defined by the relative ratio of HT-couplings, was determined by <sup>1</sup>H NMR spectroscopy (Figure 1). Due to the poor solubility of *e.g.* **P1**, the spectra were recorded in CS<sub>2</sub>/C<sub>2</sub>D<sub>2</sub>Cl<sub>4</sub> (3/1). The RR was determined by the ratio of the integration of the HT-HT triad (7.35 ppm) and that of all triad (7.35 ppm + multiple peaks around 7.15 ppm). The aromatic region of the polymers is shown in Figure 3 and the results are summarized in Table 1. They clearly confirm the regioregularity of **P1**, as only one peak is present, and increasing regio-irregularity in **P2** up to **P5**.

### Chiroptical properties in solution

The optical properties and supramolecular organization of **P1-P5** were investigated by UV-vis and CD spectroscopy. First, the UV-vis spectra of the polymers were recorded in good solvent, CHCl<sub>3</sub> (Figure 2A). Already at first sight a difference between the polymers shows up: while **P5** is readily soluble in CHCl<sub>3</sub>, **P1** (and **P2**) only dissolve on heating and the polymers partially aggregates again upon cooling. This is also expressed in the UV-vis spectra, as distinct absorption features of aggregation (near 600 nm, see also further) are present. The solution of completely dissolved **P1** (and **P2**) at room temperature can, however, be obtained in CHCl<sub>3</sub>/CS<sub>2</sub> (SI, Figure S9).  $\lambda_{\max}$  of **P1-P5** are tabulated in Table 2 and show a clear blue-shift upon decreasing RR. Note that the slightly lower  $\lambda_{\max}$  of **P1** than **P2** is due to overlapping with the aggregation peaks. In the CHCl<sub>3</sub>/CS<sub>2</sub> (4/1) solution, the  $\lambda_{\max}$  are equal (526 nm). This blue-shift is perfectly in line with the increasing amount of HH-couplings, which prevent an efficient conjugation due the twisting of consecutive thiophene units, as previously reported<sup>13</sup>.



**Scheme 1.** Synthesis of P3ASTs with different RR (P1-P5). Conditions: i) *i*-PrMgCl, THF rt; ii) 1) LDA, THF, -78°C; 2) MgBr<sub>2</sub>, THF, -78°C to rt; iii) Ni(dppp)Cl<sub>2</sub>, THF, rt.

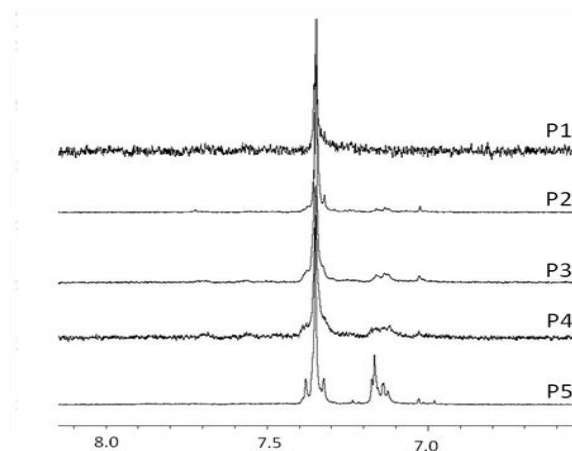


**Figure 1.** <sup>1</sup>H NMR spectrum (aromatic region) of **P1-P5** in CS<sub>2</sub>/C<sub>2</sub>D<sub>2</sub>Cl<sub>4</sub> (3/1).

Table 1. GPC data and RR of P1-P5.

P3ASTs	$\overline{M}_n$ (kg/mol)	D	RR
<b>P1</b>	14.6	1.8	~100%
<b>P2</b>	15.2	1.7	92%
<b>P3</b>	12.1	1.7	85%
<b>P4</b>	11.1	1.9	80%
<b>P5</b>	18.1	1.5	67%

Table 2. Optical properties of **P1-P5** in CHCl<sub>3</sub>.

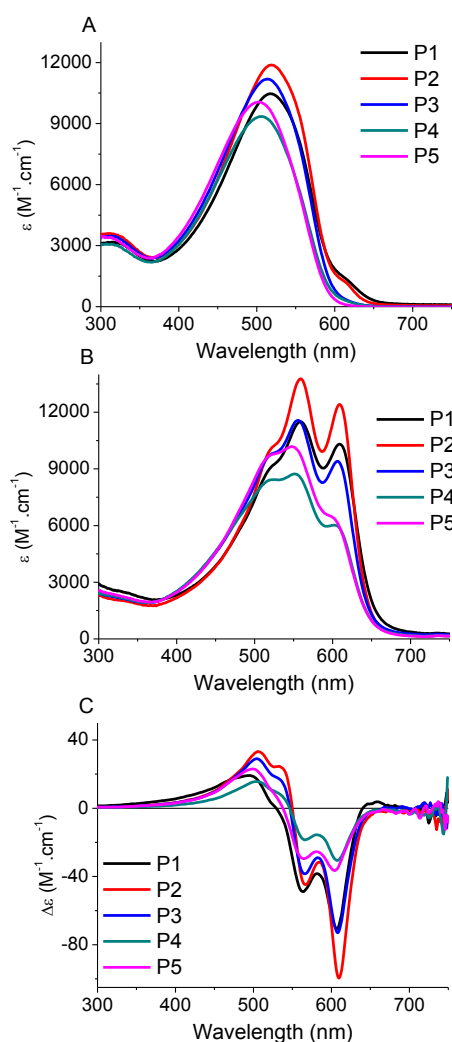
P3ASTs	$\lambda_{\max}$ (nm)	$\lambda_{\text{em}}$ (nm)	Stokes Shift (cm <sup>-1</sup> )	FWHM (cm <sup>-1</sup> )
<b>P1</b>	517	523	2482	/
<b>P2</b>	519	523	2509	/
<b>P3</b>	514	515	2723	1331
<b>P4</b>	504	509	2952	1477
<b>P5</b>	503	507	3001	1426

Next, UV-vis and CD spectra were recorded in different ratios of CHCl<sub>3</sub>/MeOH (SI, Figures S10-S14). Increasing the amount of MeOH results in aggregation of P3ASTs<sup>13</sup>. This aggregation is

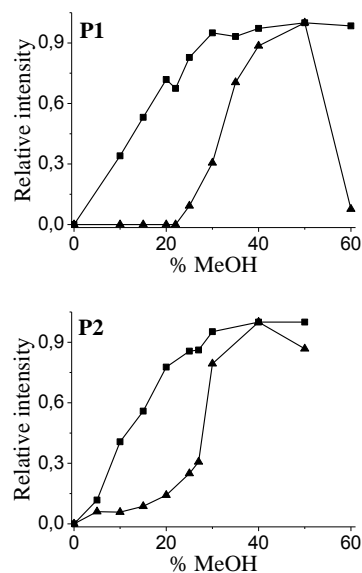
manifested by the red-shift and the occurrence of fine-structure in the absorption spectrum. The presence of clear Cotton effects demonstrates a chiral stacking. Figure 2B-C shows the UV-vis and CD spectra of **P1-P5** in a solvent mixture in which the strongest Cotton effects are observed (*i.e.* 40-55% MeOH). A first observation is that all P3ASTs, also the highly regio-irregular **P5**, form supramolecular aggregates in which chirality is expressed. Moreover, the shape of the spectra of all polymers and the position of the bands hardly differs, demonstrating that essentially the same aggregation occurs. More in particular, the fact that  $\lambda_{\text{max}}$  is equal proves that the polymer chains are equally well planarized in **P1-P5**, again showing that the energy penalty associated with steric hindrance in a planar HH-dyad of P3AST can be compensated by the gain in conjugation and  $\pi$ -stacking. Next, the solvatochromism experiments (Figures S10-S14) are examined into more detail. For this purpose, we also plotted the relative intensity of the absorption band at 610 nm as a function of MeOH content (Figures 3). It is clear that, although the aggregation occurs at a higher nonsolvent content as RR decreases. This is in line with the observed increase in solubility and reflects a lower tendency of regio-irregular P3ASTs to stack. Therefore, it can already be qualitatively concluded that although essentially the same type of aggregates are formed, a higher nonsolvent content is required as the RR decreases.

If the UV-vis and CD spectra are examined into more detail, it becomes clear that the spectra in a poor solvent mixture (Figure 2B) are in fact composed of three “chromophores”. One band (~510 nm), which is CD silent, arises from disordered, coiled polymer chains. A second transition (~540 nm, with vibronic fine-structure) is localized on planar, chirally stacked chains. This transition gives rise to bisignate Cotton effects, which originate from chiral exciton coupling of transition dipole moments located on the planar, chirally oriented polymer chains. Finally, all samples also show a red-shifted shoulder around 610 nm, with corresponding monosignate Cotton effect. This distinct, low-energy absorption band can be attributed to a helical transition dipole moment, delocalized over multiple, aggregated polymer chains<sup>28,29</sup>. Such transition was in fact already observed for other conjugated polymers as well<sup>13,30,31,9</sup>. Therefore, while the presence of the band at ~540 nm denotes planarization and (chiral) organization of the polymer backbone, the band at ~610 nm points at  $\pi$ -interactions. The presence and strength of the Cotton effects on its turn provide information on the chirality.

Already from first inspection of the UV-vis spectra (Figure 2B), it is clear that **P1-P5** differ in the intensity of the ~540 and ~610 nm peaks, which are related to the supramolecular organization. Therefore, it can already be concluded that, in contrast to our previous findings, that the supramolecular organization does in general decrease as RR drops. Interestingly, the aggregation-related absorption bands of **P2** are more intense and pronounced than of **P1**. In order to examine this into more detail, we performed a deconvolution of the UV-vis spectra in the poor solvent mixture using a linear programming method. (SI, Figures S15 A-E). Figure 4, left axis, shows the evolution of the band near ~610 nm, that probes  $\pi$ -interactions, as a function of the RR. Importantly, this clearly shows that the intensity of this band, and thus the amount and strength of  $\pi$ -interactions, does not scale linearly with the RR, but shows a maximum at high, but not 100%, RR.



**Figure 2.** UV-vis spectra of **P1-P5** in  $\text{CHCl}_3$  (A) and  $\text{CHCl}_3/\text{MeOH}$  (**P1**: 50 % MeOH, **P2**: 40 % MeOH, **P3**: 40% MeOH, **P4**: 45% MeOH, **P5**: 55% MeOH (B); and CD spectra in  $\text{CHCl}_3/\text{MeOH}$  (C).  $c_{\text{P1}}= 6.12 \cdot 10^{-5} \text{ M}$ ;  $c_{\text{P2}}= 6.04 \cdot 10^{-5} \text{ M}$ ;  $c_{\text{P3}}= 6.28 \cdot 10^{-5} \text{ M}$ ;  $c_{\text{P4}}= 6.02 \cdot 10^{-5} \text{ M}$ ;  $c_{\text{P5}}= 6.16 \cdot 10^{-5} \text{ M}$ .



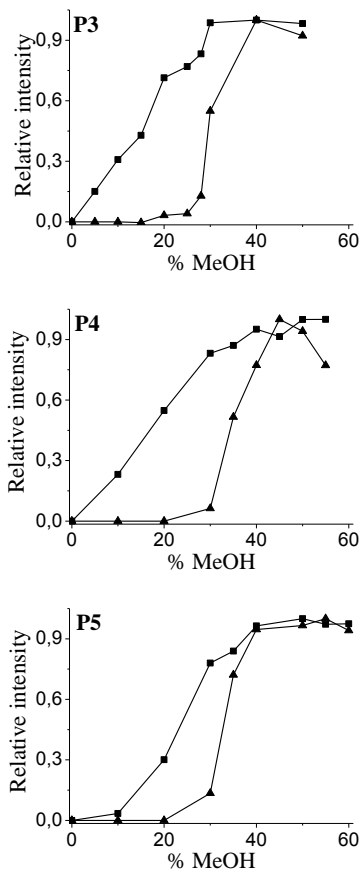


**Figure 3.** Evolution of the relative intensity of the peak at 610 nm in the UV-vis (■ -) and CD spectra (▲ -) in a CHCl<sub>3</sub>/MeOH mixture in function of the MeOH content of P1, P2, P3, P4 and P5 cP1= 6.12·10<sup>-5</sup> M; cP2= 6.04·10<sup>-5</sup> M; cP3= 6.28·10<sup>-5</sup> M; cP4= 6.02·10<sup>-5</sup> M; cP5= 6.16·10<sup>-5</sup> M.

Also the CD spectra (Figure 2B) show the same trend: in general, the intensity of the Cotton effect, reflecting chiral stacking of the polymer chains, decreases with decreasing RR, but the decrease is not linear; instead it shows an optimum at high, but smaller than 100% RR (*i.e.* P2). In order to examine the chirality of the samples, the dichroic ratio,  $g_{\text{abs}}$ -value ( $= \Delta\epsilon/\epsilon$ ), was calculated for P1-P5. If the  $g_{\text{abs}}$  remains unchanged as RR decreases, the drop of the intensity of the Cotton effects simply originates from the smaller intensity of the corresponding absorption band. Thus, in that case, while the fraction of stacked polymer chains is lower, the chiral orientation of the stacked chains remains unchanged. Conversely, if  $g_{\text{abs}}$  decreases, this means that the angle by which the polymer chains are rotated with respect to each other within the aggregates also varies (*i.e.* becomes smaller). From Figure 4, right axis, it is clear that  $g_{\text{abs}}$  decreases. Therefore, we must conclude that the amount of  $\pi$ -stacked polymer chains *and* their chiral orientation is indeed dependent on the RR, but that the relation is not linear. Instead, a small amount of regio-irregularity results in a higher fraction of stacked polymer chains which show in addition stronger Cotton effects. This can to a certain extent be correlated with the aggregation of random copoly(3-alkylthiophene) composed chiral and achiral monomers. In these polymers, the highest Cotton effects are not observed in the chiral homopolymer, although the fraction of chiral moieties is the highest, but in the copolymers<sup>32</sup>. Clearly, the introduction of some molecular asymmetry, either by the incorporation of a second

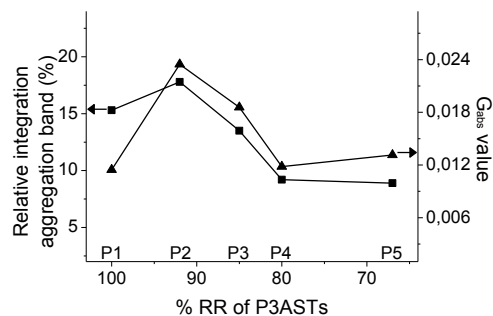


**Figure 4.** Evolution of the relative intensity of the peak at 610 nm (left) and  $g$ -value (right) in a CHCl<sub>3</sub>/MeOH mixture showing maximal Cotton effects in function of RR.

monomer (copolymerization approach) or regio-irregularity, aids in obtaining a more efficient chiral stacking. Related findings were reported by Jennheke *et al.*<sup>33</sup>. They showed that random copolythiophenes have the same supramolecular aggregation behavior as the homopolymers, but that these copolythiophenes have enhanced electronic/optoelectronic properties compared to those of the homopolymers.

These findings can explain why the previously studied regioregular and regio-irregular P3AST show very similar properties. Indeed, based on the <sup>1</sup>H NMR spectra,  $\lambda_{\text{max}}$  in CHCl<sub>3</sub> and  $\Delta\epsilon$  in CHCl<sub>3</sub>/MeOH, the regioregular polymer is similar to P1, while the regio-irregular polymer resembles P3 (or a P3AST between P3 and P4). Figure 4 confirms that such polymers indeed show very similar properties, as will also be shown by the AFM and STM experiments (see further). However, Figure 4 reveals that it must not be concluded that RR does not affect the properties of P3ASTs. The fact the previously studied regioregular and regio-irregular P3AST show similar features in their aggregated state because the RR of P<sub>irreg</sub> is such that it ‘accidentally’ has the same properties.

Next, the solvatochromism experiments are further examined. As already mentioned, in Figure 3 the relative intensity of the absorption band near 610 nm, that is related to  $\pi$ -stacking, is plotted in function of the MeOH content. For this purpose, the intensity of this absorption is divided by the maximal intensity of this absorption during the solvatochromism of each polymer. The calculations were also repeated for the CD spectra, which measures the chirality of the stacking. In fact, the magnitude of between the stacked polymer chains<sup>34,35,36</sup>. As the distance between the stacked polymer chains cannot dramatically change, the CD intensity thus reflects the angle by which the polymer chains are rotated. First, it is observed that for all P3ASTs, the evolution in the UV-vis spectra precedes the CD spectra. This shows that first aggregates composed of achirally stacked polymer chains, are formed, which, upon further increasing the nonsolvent quality, evolve to aggregates composed of chirally stacked chains. Second, it is clear that at very high nonsolvent content, the chiral response decreases again (except for P5). Such behaviour is quite commonly observed in chiral conjugated polymers<sup>28</sup> and can be ascribed to a decrease of the angle by which the polymer chains are rotated, *i.e.* they become more parallel aligned. Taken together, the evolution of the UV-vis and CD intensity as a function of the nonsolvent content shows that first aggregates are formed in which the polymer chains are hardly rotated. Regio-irregularity increases the nonsolvent content required for the stacking. Increasing the nonsolvent content results in a gradual increase of the torsion angle. Finally, at very high nonsolvent

quality the polymer chains again adopt a more parallel orientation. The latter effect is more pronounced in regioregular P3ASTs.

This behaviour can be more generally interpreted. When chiral conjugated polymers stack, two competing phenomena are at work. The first are  $\pi$ -interactions, which become stronger as the distance between the stacked chains decreases and which promote a parallel orientation. In addition, if the side-chains are organized as well, this crystallization of the side-chains is a second driving force for the stacking. The second effect is steric repulsion originating from the chiral, branched side-chains. This promotes a twisting of the stacking. The effect is small if the distance between the chains is larger, as the environment is then sterically less demanding. In regio-irregular P3ASTs, the aggregation requires a higher nonsolvent content. The main reason is that – although essentially the same type of aggregation occurs, as exemplified by the similarity of the UV-vis and CD spectra, the planarization is compromised due to the presence of HH-couplings. The number of aggregated chains is lower and  $\pi$ -interactions are less strong (less pronounced band at ~610 nm), reflecting a somewhat higher distance between the polymer chains. The steric environment around the chiral moieties is thus in general less demanding, resulting in smaller  $g_{\text{abs}}$ -values. Even at a very high nonsolvent content, the distance between the polymer chains does not become that small and consequently, the  $\pi$ -interactions so strong, that a more parallel orientation becomes again more favored. In contrast, in regioregular P3ASTs, the fraction of stacked polymer chains is higher (more intense peaks at ~540 and ~610 nm) and the  $\pi$ -interactions are slightly stronger (more pronounced band at ~610 nm), reflecting a shorter intermolecular distance. This closer packing results in a stronger steric effect of the branched substituent and consequently, a larger twisting, as evidenced by the larger  $g_{\text{abs}}$ -values. Moreover, the fact the polymer chains are more easily planarized, results in a shorter possible distance between the polymer chains at very high nonsolvent content. In this regime, the very strong  $\pi$ -interactions promote a more parallel orientation of the polymer backbones.

It might be tempting to conclude that the less steric hindrance between stacked polymer chains results in optimal crystallinity, chiral expression and  $\pi$ -stacking. However, too strong  $\pi$ -interactions can result in kinetically trapped aggregates, while in samples in which the  $\pi$ -interactions are slightly weakened, a thermodynamically favored supramolecular structure with an optimal balance of all interactions involved can be achieved. Evidence that the formation of such supramolecular structure is impeded in **P1** is provided by DSC experiments and UV-vis and CD spectroscopy in films (see below). Such fine-tuning of the  $\pi$ -interactions can be achieved by manipulating the RR. This explains why the UV-vis spectrum of **P2** in a poor solvent mixture is more defined. Moreover, the slightly weakening of  $\pi$ -interactions in **P2** also explains why stronger Cotton effects are observed: the  $\pi$ -interactions, promoting a parallel and hence achiral stacking, are weakened compared to the chiral orientated effect of the side-chains.

An interesting question that remains is whether the driving force to stack is indeed solely  $\pi$ -interactions and that the difference between **P1-P5** is due to a difference in planarization affecting the strength of the  $\pi$ -interactions, or that also an organization of the alkyl side-chains occurs. A regio-irregular placement of the substituent complicates such organization of the alkyl groups and, hence, the smaller tendency of regio-irregular P3ASTs might also (partly) be due to a reduced organization in the alkyl phase. In

order to examine this hypothesis, IR measurements were performed on powders of **P1-P5**. These samples were in fact prepared by precipitation in methanol and can therefore be considered to be similar as the aggregates studied in poor solvent mixture. McCulloch *et al.*<sup>37</sup> have already used IR spectroscopy in order to investigate whether the alkyl substituents of poly(thiophene)s are amorphous or crystalline. More in particular, the frequency of the methylene asymmetric stretch gives information about the local order of the alkyl chains. Frequencies observed around 2918  $\text{cm}^{-1}$  are an indication for ordered, all-trans alkane chains, while those around 2928  $\text{cm}^{-1}$  are an indication for liquid like alkane chains. The fact that no difference at all was observed between the IR spectra of **P1-P5** (SI, Figure S18-S22) and that the bands do not coincide with that of crystalline PE indicates that the side-chains in these (chiral) P3ASTs are not organized.  $\Pi$ -interactions are thus the sole driving force for aggregation.

Also fluorescence spectroscopy was performed. The measurements were carried out in chloroform. The polymers were excited at 500 nm. From Figure S16 and Table 2 it is clear that always the same emission is found. The emission intensity of **P1** is lower, which can be explained by the fact that the polymer is partly present in its aggregated state, in which it relaxes nonradiatively. Indeed, if the emission spectra were repeated in a mixture  $\text{CHCl}_3/\text{CS}_2$  (Figure S17), the emission intensity of **P1** becomes more intense.

The  $\lambda_{\text{em}}$  of all polymers is essentially the same. This implies that the emitting chromophore is similar, indicating that all polymers adopt the same, planar conformation in the excited state. This again confirms that a planar conformation around a HH-dyad is possible in P3ASTs. The Stokes shift, that measures the energy difference between absorption and emission, increases from **P1** up to **P5**, which reflects the blue-shift in absorption upon increasing the regio-irregularity. A similar trend is observed for broadness of the emission peak (Fwhm).

## Chiroptical behavior in film

Next, films of **P1-P5** were spincoated from chloroform solutions. For **P1** and **P2** this required mild heating. The UV-vis spectra (Figure 7) resemble those of the polymers in poor solvents, demonstrating that also in film **P1-P5** aggregate. Interestingly, also in film, the peak at ~610 nm is more pronounced for **P2**. This becomes even more clear in the CD spectra: while all polymers, including **P1**, show only minor effects, **P2** shows strong Cotton effects. Similar as in poor solvents, the CD spectrum is composed of a bisignate Cotton effect associated with transition near ~540 nm and a monosignate Cotton effect at ~610 nm. Next, the samples were annealed at 180 °C for 1 minute. This does not alter the UV-vis spectra significantly; the CD spectra, in contrast, become much more intense. The shape of the spectra remains unchanged. Importantly, also the highest Cotton effects, as determined by the  $g_{\text{abs}}$ -value, were obtained for **P2**; **P1** even showed the lowest  $g_{\text{abs}}$ -value. After repeating the experiment and cooling down the sample at a slow rate (10°C/min), no significant changes in the spectrum were observed. Clearly, the aggregation of the stiff, regioregular **P1** is kinetically impeded. This effect is more pronounced in films, in which the mobility of the polymer chains is more restricted, than in poor solvents. The fact that the  $g_{\text{abs}}$ -value of **P1** is much lower than of **P<sub>reg</sub>**, can also be attributed to the restricted mobility of **P1** due to its higher molar mass. This

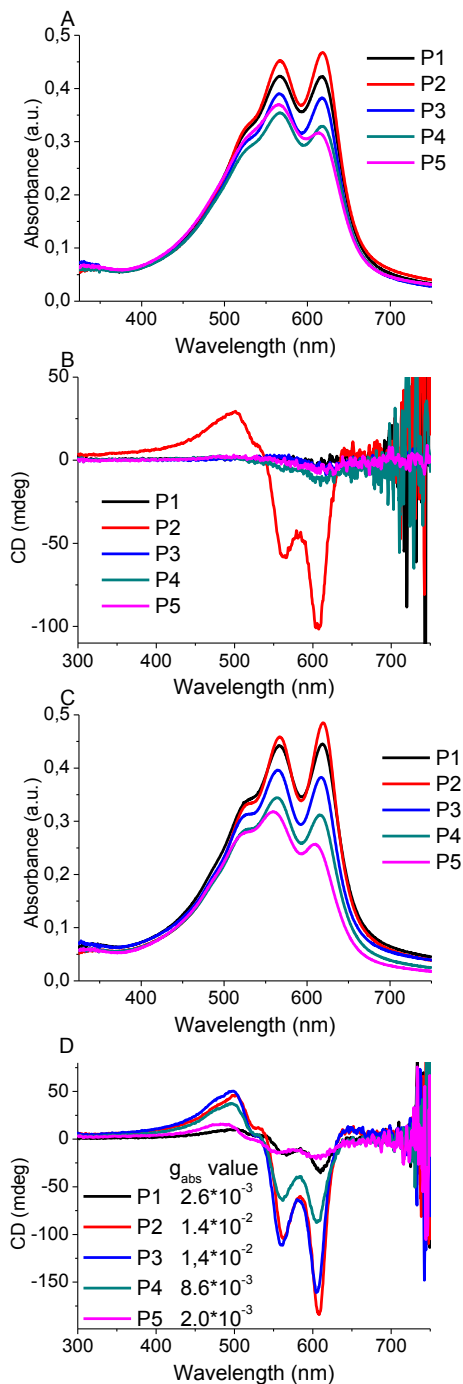


**Figure 5.** UV-vis spectra (A) and CD (B) spectra of films of **P1-P5** before and after ((C) and (D)) annealing. The samples were annealed for 1 minute at 180 °C.

can also be correlated with the poorer solubility of **P1** (see above) and DSC results (see below).

Therefore, it can be concluded from the UV-vis and CD spectra that the strongest aggregation and chiral expression is not found for the P3AST with the highest degree of regioregularity, but that a small amount of regio-irregularity facilitates the aggregation and chiral stacking.

### DSC

In order to verify the correlation between the degree of RR of

**Table 3.**  $T_m$  and  $\Delta H_m$  of **P1-P5**.

P3ASTs	$T_m$ (°C)	$\Delta H_m$ (J/g)
<b>P1</b>	/	/
<b>P2</b>	204	8.31
<b>P3</b>	204	6.48
<b>P4</b>	207	5.48
<b>P5</b>	190	3.57

P3ASTs and the crystallinity, some DSC experiments were performed. All polymers are semi-crystalline and show similar thermograms, suggesting that the same type of crystals is formed. The melting temperature  $T_m$  and melting enthalpy ( $\Delta H_m$ ) were typically measured at the second heating run and are shown in Table 2. **P1** did not show a melting peak in the second scan. Clearly, the crystallization of **P1** is kinetically restricted, which is also in line with the UV-vis and CD results of films of **P1**. Very slow cooling (1°C/min) or annealing did not result in any crystallization. In general,  $T_m$  and  $\Delta H_m$  decrease with increasing RR, which is in line of the observations of UV-vis and CD spectroscopy. Since the melting of **P1** could not be measured, the tendency observed with the chiroptical techniques – the highest tendency to aggregate is found for high, but not the highest degree of RR - could not be verified.

### STM

Having established the influence of the RR on the supramolecular behaviour and chiroptical properties in P3AST, a plausible explanation why the previously studied regioregular and regio-irregular P3AST show very similar properties. In order to test whether these polymers show indeed the same structure in solid state, we used STM and AFM to obtain real space visualization. STM imaging was done on polymer samples dropcasted on graphite. STM is a high-resolution imaging technique that can provide very high spatial resolution, close to the atomic scale, of thin molecular or polymer films (typically one monolayer thick), on atomically flat conductive substrates such as graphite. High-resolution imaging is possible under ambient conditions and at the liquid-solid interface, and it has been demonstrated before that STM can provide high-resolution images of certain classes of polymers, and in particular polythiophenes. Mena-Osteritz *et al.* were the first to provide direct visualization of polymer folds in submolecular resolution of two-dimensional crystals of head-to-tail coupled poly(3-alkyl-thiophene)s<sup>14</sup>. Inspiring subsequent work includes studies on head-to-tail coupled poly(3-alkylthiophene)s<sup>15-19</sup>, oligothiophenes<sup>20,21</sup>, regioregular alternating  $\pi$ -conjugated copolymers<sup>22</sup>, and the surface-assisted electrochemical synthesis of polythiophenes<sup>23,24</sup>. In this work, the samples were prepared by depositing a saturated solution of the polymer in 1,2,4-trichlorobenzene on graphite. A representative STM image of both polymers is shown in Figure 6. It is clear that both polymers nicely organize into domains, with the typical domain size being around 1400 nm<sup>2</sup> for both polymers.. Fourier analysis (Figure S1) reveals that mainly three directions are favored, reflecting the influence of the substrate on the self-assembly process. Careful data analysis shows that the polymer backbones actually align along six rather than three directions. The angle between the backbones of nearly parallel domains is 8°,

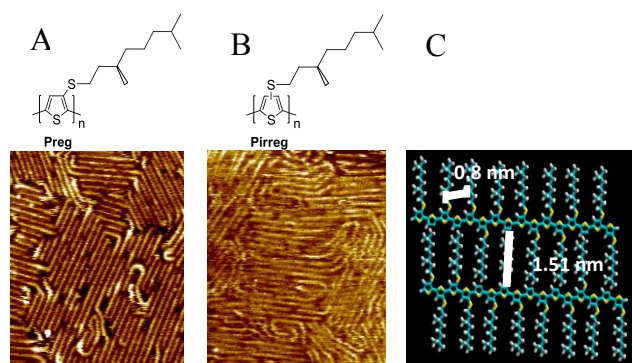


**Figure 6.** Representative STM image of the self-assembly of  $P_{reg}$  (A) and  $P_{irreg}$  (B) at the 1,2,4-TCB/graphite interface and a representation of the organized polymer chains with only some of the alkyl chains adsorbed. (C). (A) Size STM image is  $39.3 \times 46.2 \text{ nm}^2$ .  $I_{set}=127 \text{ pA}$ ,  $V_{set}=-860 \text{ mV}$ . (B) Size STM image is  $42.1 \times 42.1 \text{ nm}^2$ .  $I_{set}=189 \text{ pA}$ ,  $V_{set}=-680 \text{ mV}$

with a deviation from the graphite main symmetry axes of  $+4^\circ \pm 1$  or  $-4^\circ \pm 1$ . Both deviations are equally presented, demonstrating that despite the presence of a chiral substituent, the chiral nature of the alkoxy chains does not lead to monolayers with a clear chiral character. The distance between two adjacent substituents is 0.8 nm, rendering interdigitation of the substituents impossible. The distance between two polymer chains is  $\pm 1.5 \text{ nm}$ , which is too short for noninterdigitated chains to lay flat on the substrate. Instead, some (parts of the) side chains must still be in solution. This is also in line with the absence of chirality in the STM images, as the chiral side-chains do not participate in the organization. Alternatively, the side chains can be tilted with respect to the conjugated backbone, instead of being perpendicular to it, resulting in a distance of 1.5 nm. It was not possible to discriminate between those two possibilities, even with the use of high-resolution STM.

Upon close inspection, two differences between the regioregular and regio-irregular polymer become clear. First, the monolayers of the regioregular polymer are more ordered. This is revealed by the Fourier transformations on the pictures (Figure S1). Therefore, it must be concluded that, although some substituents are not adsorbed and chirality is not expressed, the irregular nature of regio-irregular polymer complicates the adsorption, resulting in a larger spread of the orientations of the polymer chains with respect to the major symmetry axis of graphite. In this respect, it is interesting to note that the regioregular P3AST immediately self-assembled into organized structures, while for regioirregular polymer self-assembly on the surface was more difficult (*i.e.*, required longer times).

The second difference is related to the molar mass of both polymers. The length of a representative set of polymer chains was determined and summarized in histograms (Figures S2). It is clear that the regioregular polymer is composed of longer chains than its regioregular counterpart, which is perfectly in line with the larger molar mass as determined by GPC ( $\overline{M}_n=17.5 \text{ kg/mol}$  versus  $9.6 \text{ kg/mol}$ ). Interestingly, the histograms allow for an absolute determination of the molar mass and polydispersity (PDI) of the two polymers. These calculations reveal for the regioregular polymer  $\overline{M}_n=12.6 \text{ kg/mol}$  and  $\text{PDI}=1.4$  (GPC:  $\overline{M}_n=9.6 \text{ kg/mol}$  and  $\text{PDI}=1.6$ ) and for the regio-irregular counterpart  $\overline{M}_n=17.3 \text{ kg/mol}$  and  $\text{PDI}=1.3$  (GPC:  $\overline{M}_n=17.5 \text{ kg/mol}$  and  $\text{PDI}$

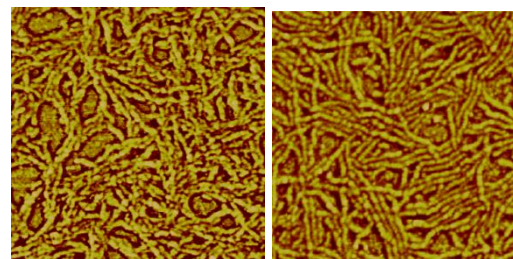


**Figure 7.**  $1 \times 1 \mu\text{m}^2$  tapping-mode AFM phase images of thin deposits of the regioregular (left) and regioirregular (right) P3AST. The vertical color code corresponds to 40 degrees.

$= 1.4$ ). This would suggest that GPC underestimates the molar mass when calibrated towards poly(styrene), which is in contrast with the fact that the molar mass of stiffer polymer samples is overestimated when calibrated with more flexible standards. Most likely, the longer chains adsorb preferentially, since they would benefit more from intermolecular interactions with the substrate. As a result, the molecular weight distributions determined from the STM data are likely to be biased towards higher molecular weights, which would then explain the discrepancy with respect to the GPC data.

## AFM

The microscopic morphology of thin deposits of both P3ASTs was examined with AFM; representative images are presented in Figure 7. It clearly appears that both polymers give rise to a fibrillar morphology. Such an organization is very often observed in thin films of P3ATs<sup>25,26</sup>; it originates from the  $\pi$ -stacking of the conjugated backbones, in such a way that the chains are perpendicular to the fibril axis and the plane of the conjugated backbone is perpendicular to the substrate. In other words, the chains are adsorbed ‘edge-on’ the glass, a substrate that does not favor the flat adsorption of the chains observed with STM on graphite. The similarity between the two images indicates that the capacity of P3AST chains to aggregate into well-defined assemblies is not significantly affected by the regioregularity of the polymer, at least down to the degree of regioregularity present in used regio-irregular P3AST. This is fully consistent with the UV-vis absorption and CD spectra as well as with the DSC data. It is also noteworthy that the average width of the fibrils is similar for the two polymers ( $21.3 \pm 3.6 \text{ nm}$  in the regioregular polymer vs.  $20.8 \pm 1.7 \text{ nm}$  in the regio-irregular one). Given the fact that the molar mass of the two polymers is significantly different, this shows that the crystals are self limiting, similar as P3ATs. In summary, both STM and AFM confirm the strong similarity between the previously studied regioregular and regio-irregular P3AST.

## Conclusion

In the first part of the manuscript, a series of P3ASTs (**P1-P5**) with different RR was synthesized with  $\text{Ni}(\text{dppp})\text{Cl}_2$  as a catalyst. The RR was changed by varying the isomeric purity of the monomers feed (**2a'** and (**2a** + **2b**)). The difference in RR was verified and estimated by  $^1\text{H}$  NMR spectroscopy. In good solvent all the polymers adopt a coil like structure with a blue shift for the polymers with a lower degree of RR, due to the increasing amount of HH couplings which cause twists between two consecutive thiophenes units. Emission spectroscopy showed that all the

polymers have a similar emitting chromophore, indicating that all the polymers adopt the same, planar conformation in the excited state. In poor solvents or films, **P1-P5** form supramolecular aggregates in which the driving force to stack are solely the  $\pi$ -interactions. The chiral orientation ( $g_{\text{abs}}$ -value) and amount of  $\pi$ -stacked polymers do depend on the degree of RR. Interestingly, this dependence is not linear: the strongest aggregation and chiral expression is not found in the most RR P3ASTs, but in those with a small amount of regio-irregularity, indicating that a small amount of molecular disorder facilitates the aggregation and chiral stacking. Due to the fact that there is not a linear, but a non-monotonic relationship between RR and aggregation behavior, it can be explained why previously studied regioregular and regio-irregular P3AST show similar features in their aggregated state.

Next, a thorough investigation on their capacity of self-assembling of the previously studied regioregular and regio-irregular P3AST was performed. The STM study showed that both polymers have the same tendency to organize on graphite. The only, albeit small, difference observed, was the degree of order in the monolayers, in which the regio-irregular P3AST exhibits more disorder. Consistently, AFM data show that the two polymers have a tendency to organize into fibrillar supramolecular assemblies in a very similar way.

## Materials and Methods

### Instrumentation

Gel permeation chromatography (GPC) measurements were done with a Shimadzu 10A apparatus with a tunable absorbance detector and a differential refractometer in tetrahydrofuran (THF) as eluent toward polystyrene standards.

UV-vis and CD spectra were recorded with a Varian Cary 400 and a JASCO 62 DS apparatus respectively. The DSC experiments were performed on a DSC 7 from Perkin Elmer

Films were prepared by spincoating from chloroform solutions on a glass substrate. An equal polymer concentration (11.3 mg/mL) was used for **P1-P5** and the preparation parameters were kept constant for (spinning speed: 1500 rpm; spinning time: 30 s). A Mettler-Toledo FP900 Thermosystem was used for sample annealing. Polymer films were heated at 180°C for one minute.

Prior to the STM imaging, the polymer was dissolved in 1,2,4-trichlorobenzene (TCB) (Sigma-Aldrich >99%). A droplet of the solution was applied onto a freshly cleaved surface of highly oriented pyrolytic graphite (HOPG, grade ZYB, Advanced Ceramics Inc., Cleveland, OH), and the STM imaging was performed at the interface between HOPG and TCB. STM-experiments were performed on a Molecular Imaging PicoSPM (Agilent). The tips were mechanically cut from Pt/Ir wire (80%/20%, diameter 0.2 mm). The STM-images were obtained in the constant current mode. For analysis, images of the graphite substrate underneath the monolayer were recorded immediately after recording an image of the monolayer. The images were corrected for drift with scanning probe image processor (SPIP) software (Image Metrology ApS) using the recorded graphite images for calibration purposes. The imaging parameters are indicated in the figure captions: tunneling current  $I_{\text{set}}$  and sample bias  $V_{\text{set}}$ .

The thin deposits for AFM studies were prepared from solutions of **P<sub>reg</sub>** and **P<sub>irreg</sub>** in chlorobenzene at a concentration of 0.2 mg/mL. The deposits were generated by drop-casting 25  $\mu\text{L}/\text{cm}^2$  of the solution on glass substrates and letting the solvent

evaporate overnight in a solvent-saturated atmosphere. The AFM measurements were carried out in ambient conditions, with a Bruker Multimode microscope equipped with a Nanoscope V controller. The microscope was operated in intermittent-contact mode, using commercially available silicon tips with a spring constant of 42 N/m, a resonance frequency of about 330 kHz and a typical radius of curvature in the 5-10 nm range. Both the height and phase signals were recorded, with a 512x512 pixels resolution. The images are presented as recorded, except for a plane-fitting processing.

Compound **1** and **3** were synthesized as described in the literature<sup>13</sup>.

### Synthesis of P1-P5.

**In situ synthesis of (+)-2-bromo-5-bromomagnesio-4-((S)-3,7-dimethyl-octylsulfanyl)thiophene and (+)-5-bromo-2-bromomagnesio-4-((S)-3,7-dimethyloctylsulfanyl)thiophene 2a + 2b.**

To a solution of **1** (1.50 mmol; 621 mg) in THF (10 ml) was added *i*-PrMgCl (2M solution in THF; 1.50 mmol; 750  $\mu\text{l}$ ) at 0°C and under an argon atmosphere and the mixture was stirred for 30 minutes. Before starting the polymerization an aliquot (200  $\mu\text{l}$ ) was withdrawn from the solution, poured into D<sub>2</sub>O and analyzed with <sup>1</sup>H NMR spectroscopy to determine the ratio of both isomers; 45% for **2a** and 40% for **2b**, the remainder consists of 3-((S)-3,7-dimethyl-octylsulfanyl)thiophene (SI, Figure S3).

**In situ synthesis of (+)-2-bromo-5-bromomagnesio-4-((S)-3,7-dimethyl-octylsulfanyl)thiophene 2a'.**

A solution of **3** (1.50 mmol; 503 mg) in THF was cooled to -78°C and purged with argon. Lithium diisopropylamide (LDA) was added at -78°C and further stirred for 30 minutes. [LDA was prepared by dropwise addition of *n*-BuLi (2.5 M in hexane; 1.58 mmol; 630  $\mu\text{l}$ ) to a solution of (*i*-Pr)<sub>2</sub>NH (1.65 mmol; 233  $\mu\text{l}$ ) in THF (10 ml) at 0°C under argon atmosphere. The solution was further stirred at -78° for 30 minutes.] At -40° C this mixture was added to a MgBr<sub>2</sub> solution in THF (14ml) under an argon atmosphere and the reaction mixture was further stirred for another 30 minutes at room temperature [The anhydrous MgBr<sub>2</sub> solution was prepared by drop wise addition of 1,2-dibromoethane (3.00 mmol; 259  $\mu\text{l}$ ) to a suspension of Mg (3.30 mmol; 80.2 mg) in THF. The mixture was refluxed for 2h.]. Before starting the polymerization an aliquot (200  $\mu\text{l}$  of the reaction mixture) was withdrawn from the solution, poured into D<sub>2</sub>O and analyzed with <sup>1</sup>H NMR spectroscopy to verify the purity of the monomer (SI, Figure S3). This revealed that the sample consists of 60% **2a'**; the remainder being 3-((S)-3,7-dimethyl-octylsulfanyl)thiophene

### General procedure for the polymerization of P1-P5.

To a suspension of NidpppCl<sub>2</sub> (10.0  $\mu\text{mol}$ ; 5.30 mg) in THF (3ml) was added a mixture of both isomers **2a'** and (**2a+2b**). The reaction was stirred overnight at room temperature. After polymerization the reaction mixture were concentrated and the polymers were precipitated in methanol. These polymers were further purified via Soxhlet extractions using acetone, hexanes (**P1-P3**) or pentane (**P4-P5**). In a last step the polymers were extracted with chloroform, concentrated and precipitated in methanol.

**P1: 2a'** (0.35 mmol); yield = 80.2 mg (88%),

**P2: 2a'** (0.28 mmol) and (**2a + 2b**) (0.085 mmol); yield = 62.4 mg (67%),

**P3: 2a'** (0.21 mmol) and (**2a + 2b**) (0.17 mmol); yield = 79.0 mg (81%),

**P4: 2a'** (0.048 mmol) and **(2a + 2b)** (0.34 mmol); yield = 65.5 mg (66%),

**P5: (2a + 2b)** (0.43 mmol); yield = 59.8 mg (55%).

## Acknowledgments.

We are grateful to the Onderzoeksfonds KU Leuven/ Research Fund KU Leuven, the Fund for Scientific Research (FWO-Vlaanderen), the Belgian Science Office of the Federal Government (BELSPO-IAP program), the OPTI2MAT Excellence Programme of Région Wallonne, the FNRS-FRFC, KU Leuven (GOA) and the Institute for the Promotion of Innovation by Science and Technology for financial support. D.M. is grateful to FRIA for a doctoral fellowship. P.L. is research associate of the National Fund for Scientific Research (FNRS).

## Notes and references

<sup>a</sup> Laboratory of Polymer Synthesis, KU Leuven, Celestijnenlaan 200F, B-3001 Heverlee, Belgium Tel. +32 (0) 16 32 74 20 Fax. +32 (0) 16 32 79 90 e-mail: guy.koeckelberghs@chem.kuleuven.be

<sup>b</sup> Laboratory for Chemistry of Novel Materials, University of Mons – UMONS, Place du Parc 20, B-7000 Mons, Belgium

<sup>c</sup> Laboratory of Photochemistry and Spectroscopy, KU Leuven, Celestijnenlaan 200F, B-3001 Heverlee, Belgium

† Electronic Supplementary Information (ESI) available: STM images, <sup>1</sup>H-NMR, UV-vis, CD and IR spectra of the polymers. See DOI: 10.1039/b000000x/

1. M. M. Bouman and E. W. Meijer, *Adv. Mater.*, 1995, **7**, 385-387.
2. B. M. W. Langeveld-Voss, M. P. T. Christiaans, R. A. J. Janssen, and E. W. Meijer, *Macromolecules*, 1998, **31**, 6702-6704.
3. G. Bidan, S. Guillerez, and V. Sorokin, *Adv. Mater.*, 1996, **8**, 157-160.
4. B. M. W. Langeveld-Voss, D. Beljonne, Z. Shuai, R. A. J. Janssen, S. C. J. Meskers, E. W. Meijer, and J.-L. Brédas, *Adv. Mater.*, 1998, **10**, 1343-1348.
5. G. Lakhwani, G. Koeckelberghs, S. C. J. Meskers, and R. A. J. Janssen, *Chem. Phys. Lett.*, 2007, **437**, 193-197.
6. M. Lemaire, D. Delabouglise, R. Garreau, A. Guy, and J. Roncali, *J. Chem. Soc., Chem. Commun.*, 1988, 658.
7. V. Rodriguez, G. Koeckelberghs, and T. Verbiest, *Chem. Phys. Lett.*, 2007, **450**, 76-79.
8. C. R. Snyder, J. S. Henry, and D. M. DeLongchamp, *Macromolecules*, 2011, 7088-7091.
9. M. Vangheluwe, T. Verbiest, and G. Koeckelberghs, *Macromolecules*, 2008, **41**, 1041-1044.
10. D. Iarossi, A. Mucci, L. Schenetti, R. Seeber, F. Goldoni, M. Affronte, and F. Nava, *Macromolecules*, 1999, **32**, 1390-1397.
11. G. Koeckelberghs, M. Vangheluwe, C. Samyn, A. Persoons, and T. Verbiest, *Macromolecules*, 2005, **38**, 5554-5559.
12. G. Koeckelberghs, M. Vangheluwe, K. V. Doorselaere, E. Robijns, A. Persoons, and T. Verbiest, *Macromol. Rapid Commun.*, 2006, **27**, 1920-1925.
13. S. Vandeleene, K. Van den Bergh, T. Verbiest, and G. Koeckelberghs, *Macromolecules*, 2008, **41**, 5123-5131.
14. E. Mena-Osteritz, A. Meyer, B. Langeveld-Voss, R. Janssen, E. Meijer, and P. Bäuerle, *Ang. Chem. Int. Ed.*, 2000, **39**, 2679-2684.
15. B. Grévin, P. Rannou, R. Payerme, A. Pron, and J.-P. Travers, *Adv. Mater.*, 2003, **15**, 881-884.
16. M. Dubois, S. Latil, L. Scifo, B. Grévin, and A. Rubio, *J Chem Phys*, 2006, **125**, 34708.
17. L. Scifo, M. Dubois, M. E. L. Brun, P. Rannou, S. Latil, A. Rubio, and B. Grévin, *Nano Lett.*, 2006, **6**, 1711-1718.
18. G. Koeckelberghs, C. Samyn, A. Miura, S. De Feyter, F. C. De Schryver, S. Sioncke, T. Verbiest, G. de Schatzen, and A. Persoons, *Adv. Mater.*, 2005, **17**, 708-712.
19. P. Keg, A. Lohani, D. Fichou, Y. M. Lam, Y. Wu, B. S. Ong, and S. G. Mhaisalkar, *Macromol. Rapid Commun.*, 2008, **29**, 1197-1202.
20. Z.-Y. Yang, H.-M. Zhang, C.-J. Yan, S.-S. Li, H.-J. Yan, W.-G. Song, and L.-J. Wan, *P. Natl. Acad. Sci. USA*, 2007, **104**, 3707-3712.
21. Z.-Y. Yang, H.-M. Zhang, G.-B. Pan, and L.-J. Wan, *ACS Nano*, 2008, **2**, 743-749.
22. M. Brun, R. Demadrille, P. Rannou, A. Pron, J.-P. Travers, and B. Grévin, *Adv. Mater.*, 2004, **16**, 2087-2092.
23. H. Sakaguchi, H. Matsumura, and H. Gong, *Nat Mater*, 2004, **3**, 551-557.
24. H. Sakaguchi, H. Matsumura, H. Gong, and A. M. Abouelwafa, *Science*, 2005, **310**, 1002-1006.
25. M. Surin, P. Leclère, R. Lazzaroni, J. D. Yuen, G. Wang, D. Moses, A. J. Heeger, S. Cho, and K. Lee, *Journal of Applied Physics*, 2006, **100**, 033712.
26. H. Sirringhaus, P. J. Brown, R. H. Friend, M. M. Nielsen, K. Bechgaard, B. M. W. Langeveld-Voss, A. J. H. Spiering, R. A. J. Janssen, E. W. Meijer, P. Herwig, and D. M. de Leeuw, *Nature*, 1999, **401**, 685-688.
27. R. S. Loewe, P. C. Ewbank, J. Liu, L. Zhai, and R. D. McCullough, *Macromolecules*, 2001, **34**, 4324-4333.
28. S. Zahn and T. M. Swager, *Angew. Chem. Int. Ed.*, 2002, **41**, 4225-4230.
29. F. Babudri, D. Colangiuli, L. Di Bari, G. M. Farinola, O. Hassan Omar, F. Naso, and G. Pescitelli, *Macromolecules*, 2006, **39**, 5206-5212.
30. P. Brown, D. Thomas, A. Köhler, J. Wilson, J.-S. Kim, C. Ramsdale, H. Sirringhaus, and R. Friend, *Phys. Rev. B.*, 2003, **67**, 1-16.
31. S. Vandeleene, M. Jivanescu, A. Stesmans, J. Cuppens, M. J. Van Bael, T. Verbiest, and G. Koeckelberghs, *Macromolecules*, 2011, **44**, 4911-4919.
32. M. Verswyvel, F. Monnaie, and G. Koeckelberghs, *Macromolecules*, 2011, **44**, 9489-9498.
33. P.-T. Wu, G. Ren, and S. a. Jenekhe, *Macromolecules*, 2010, **43**, 3306-3313.
34. D. Cornelis, H. Peeters, S. Zrig, B. Andrioletti, E. Rose, T. Verbiest, and G. Koeckelberghs, *Chem. Mater.*, 2008, **20**, 2133-2143.
35. Alison Rodger and Bengt Nordén, *circular dichroism and linear dichroism*, Oxford University Press, 1997.
36. Purdie N., *Analytical Applications of Circular Dichroism - Elsevier*, Elsevier Science Ltd, 1993.
37. R. J. Kline, D. M. DeLongchamp, D. a. Fischer, E. K. Lin, L. J. Richter, M. L. Chabinyc, M. F. Toney, M. Heeney, and I. McCulloch, *Macromolecules*, 2007, **40**, 7960-7965.

## TOC

The supramolecular organization of poly(3-alkylsulfanylthiophene)s is optimal at high, but not 100% degree of regioregularity

